PYRITE GEOCHEMISTRY IN THE NORTH ARM EPITHERMAL Ag–Au DEPOSIT, QUEENSLAND, AUSTRALIA: A PROTON-MICROPROBE STUDY

WILLIAM L. GRIFFIN

CSIRO Division of Exploration Geoscience, Box 136, North Ryde, New South Wales 2113, Australia

PAUL M. ASHLEY

Department of Geology and Geophysics, University of New England, Armidale, New South Wales 2351, Australia

CHRIS G. RYAN, SOEY H. SIE AND GARY F. SUTER

CSIRO Division of Exploration Geoscience, Box 136, North Ryde, New South Wales 2113, Australia

ABSTRACT

The North Arm epithermal Ag–Au deposit, in Queensland, Australia, contains pyrite that displays spectacular fine-scale cryptic zoning defined mainly by arsenic content; some grains and zones contain up to 6 wt.% As. Proton-microprobe analysis shows evidence of widely variable concentrations of Cu, Sb, Se, Ag, Zn, Pb and Mo. Au contents are below detection limits (10–30 ppm), even in grains with inclusions of electrum. Cu, Sb and Se are broadly correlated with As, and with precious-metal grades in drill-core intervals. High contents of As require either the deposition of a metastable arsenian pyrite, which also accepts high levels of other elements, or a submicroscopic mixture of pyrite and other phases. Interelement correlations are consistent with a mixture of pyrite, arsenopyrite and a sulfosalt phase. The zoning of the pyrite may reflect rapid changes in fluid composition due to repeated boiling in the near-surface environment, but may also reflect chaotic behavior of very local subsystems.

Keywords: pyrite, geochemistry, Ag–Au ores, trace elements, proton microprobe, North Arm deposit, epithermal gold, Queensland, Australia.

SOMMAIRE

Le gisement épithermal à Ag–Au de North Arm, au Queensland en Australie, contient de la pyrite qui montre une zonation cryptique fine très frappante, qui résulte surtout de la distribution de l'arsenic. Dans certains grains et certaines zones, la teneur en As peut atteindre 6% en poids. Les analyses par microsonde protonique démontrent la grande variabilité en teneurs de Cu, Sb, Se, Ag, Zn, Pb et Mo. Les teneurs en Au ne dépassent pas le seuil de la détection (10–30 ppm), même dans les grains à inclusions d'électrum. Les teneurs en Cu, Sb et Se montrent une corrélation approximative avec l'arsenic, et avec les teneurs en métaux précieux dans certains intervalles dans les carottes. Les concentrations élevées en As supposent la formation d'une pyrite métastable enrichie en arsenic qui accepterait aussi les niveaux élevés des autres éléments, ou la déposition d'un mélange sub-microscopique de pyrite et d'autres phases. Les corrélations inter-éléments concordent avec l'hypothèse d'un mélange de pyrite, arsénopyrite et un sulfosel. La zonation de la pyrite pourrait résulter des changements rapides dans la composition de la phase fluide dus à son ébullition répétée dans ce milieu à faible profondeur, ou bien du comportement chaotique de sous-systèmes très locaux.

(Traduit par la Rédaction)

Mots-clés: pyrite, géochimie, minerai à Ag–Au, éléments traces, microsonde protonique, gisement de North Arm, or épithermal, Queensland, Australie.

INTRODUCTION

Pyrite is one of the most abundant sulfides in the alteration haloes and vein-stockwork mineralization of epithermal precious-metal deposits and modern geothermal systems. In some epithermal and geothermal systems, pyrite may contain up to several % As (e.g., Christiansen et al. 1983, Glaser 1986, Fleming et al. 1986, Ballantyne & Moore 1988), as well as smaller concentrations of elements such as Sb, Au, Ag, Se and Cu. In the absence of discrete arsenic-bearing phases, e.g., orpiment, realgar or arsenopyrite, arsenian pyrite is probably the main cause of primary As dispersion haloes about epithermal systems. These primary haloes and their secondary dispersion haloes are commonly used as exploration pathfinders (e.g., Ballantyne & Moore 1988, Plant et al. 1989, Elliott & Towsey 1989).

Preliminary electron-microprobe studies of the North Arm epithermal Au–Ag deposit in southeast Queensland, Australia (Ashley 1987) showed that the hydrothermal pyrite contains widely variable levels of As, and trace amounts of Cu, Zn, Ag, Sb and Se. The spatial variations of these trace elements within single grains and across the deposit contain potentially useful genetic information, and have implications for exploration strategies. However, the contents of these elements lie in most cases near the limits of detection in routine electron-microprobe studies. We have therefore carried out a more detailed study using the proton microprobe, which provides rapid, accurate, non-destructive analysis at ppm levels for most of the elements in question; with a spatial resolution on the order of 20–30 μm, it is therefore ideally suited to a study of this type.

The primary aim of this study has been to characterize the trace-element variation in the pyrite of the North Arm deposit, and to assess the causes of this variation. A secondary goal has been to examine the relation between the geochemistry of disseminated pyrite and precious-metal mineralization, and to evaluate the use of such data in exploration.

GEOLOGY OF THE NORTH ARM DEPOSIT

The North Arm epithermal deposit (Fig. 1; Ashley 1987, Ashley & Andrew 1990) occurs within the Triassic North Arm Volcanics, a gently deformed continental margin sequence of rhyolitic, dacitic and andesitic lavas, shallow intrusive bodies, and fragmental and epiclastic rocks of high-K calc-alkaline affinities. Precious metal mineralization occurs in a system of subparallel, steeply dipping fissure veins and associated minor stockworks and hydrothermal breccias. An alteration zone 3 km long and up to 1 km wide encloses the mineralization. Alteration
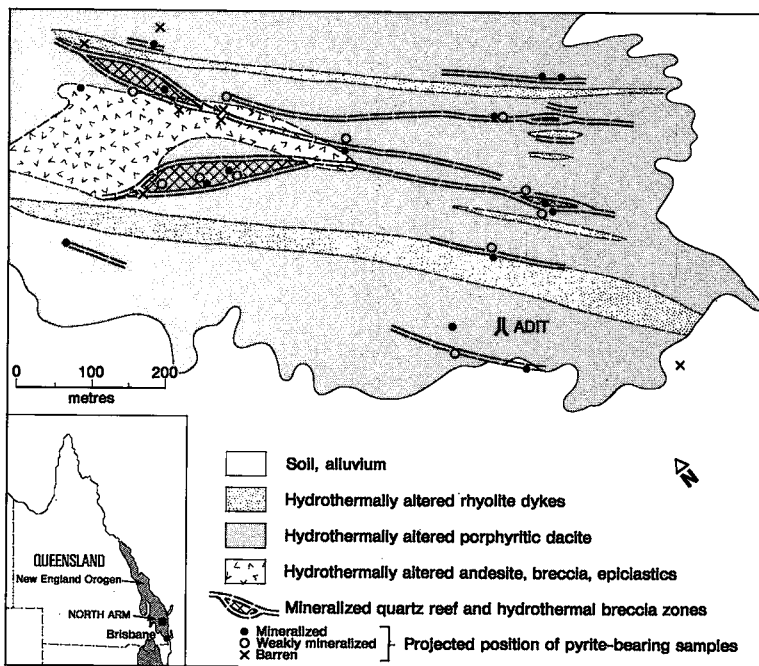

FIG. 1. Location and geology of the North Arm Au–Ag deposit, southeastern Queensland, showing locations of pyrite samples (projected to the surface).

assemblages are zoned from peripheral propylitic to phyllic and local proximal potassic–phyllic. Geological, mineralogical, geochemical and stable isotope data indicate that the deposit is of the low-sulfur adularia–sericite type of Hayba *et al.* (1985) and Heald *et al.* (1987).

Mineralized structures typically show precious metal values in the range 0.1–10 ppm Au and 1–80 ppm Ag, contained in a quartz-rich assemblage with minor calcite, sericite, pyrite and marcasite. Trace minerals include freibergite, naumannite, silver-electrum (0–64% Au), base metal sulfides and arsenopyrite. Fluid-inclusion data, mineral compositions and phase relations suggest that mineralization occurred at temperatures of 220–340°C. The hydrothermal fluids were dilute, near-neutral, CO_2-bearing, and boiling; stable-isotope data (Ashley & Andrew 1990) indicate that the fluids were dominated by meteoric water. Indications of boiling include fluid inclusions with widely varying liquid–vapor ratios, hydrothermal brecciation, colloform banded and vuggy quartz veins, and bladed calcite crystals or their pseudomorphs. Assuming hydrostatic conditions, the evidence of boiling suggests that the present level of erosion represents exhumation of the fossil geothermal system to a depth of 500–600 m.

Geochemical surveys reveal the existence of both primary and secondary dispersion haloes involving Au, Ag and As; the As haloes cover essentially the entire hydrothermally altered area (Fig. 1).

PETROGRAPHIC RELATIONS

Structures that host precious metal mineralization at North Arm contain a sparse but diverse assemblage of disseminated minerals (see above), in which the maximum grain-size of silver and naumannite is *ca.* 2.5 mm. Pyrite, the most abundant sulfide, occurs as anhedral to locally euhedral grains that range from a few μm to about 1 mm across. It occurs in three texturally distinct forms. Type A: Subhedral to euhedral, smooth-polishing grains up to 1 mm. The grains commonly are cryptically zoned and may contain inclusions up to tens of μm across of marcasite, rutile, electrum, silver, apatite, chalcopyrite, sphalerite, galena and pyrrhotite (Fig. 2a). Such pyrite commonly shows weak anisotropism (*cf.* Spry & Gredlinske 1987), with reddish to greenish tints. Type B: Domains of bladed form, commonly pitted and finely intergrown with marcasite; these may be overgrown by type A. Pyrrhotite is retained rarely in the central zone of some bladed aggregates, and the pyrite–marcasite may be in part pseudomorphous (Fig. 2b). Type C: Irregular to globular aggregates of fine-grained pyrite, commonly intergrown with marcasite and with tiny inclusions of silver minerals, base metal sulfides and arsenopyrite. This type shows

cryptic zoning, and may overgrow types A and B, or occur as disseminations in quartz (Fig. 2c).

Pyrite and marcasite commonly display growth zoning; this is not visible on freshly polished surfaces, but becomes evident after etching or exposure to air for a few weeks. The zoning is spectacularly illustrated on back-scattered electron images, and primarily reflects variations in arsenic content (Figs. 2a–c). In general, internal zones of lowest As content occur in type-A pyrite, and type-C aggregates have the highest As contents. In detail, however, there is much variation in As content at the percent level, even in type-A pyrite (Fig. 2a). The growth of pyrite grains was obviously episodic and irregular in nature, with early growth-zones being resorbed and truncated by later ones. Individual As-rich and As-poor zones in pyrite and marcasite occur on scales down to 1 μm or less (Fig. 2b). Similar zoning, in pyrite from a variety of environments, is described by Fleet *et al.* (1989).

ANALYTICAL METHODS

The HIAF proton microprobe is based on a Tandetron tandem electrostatic accelerator, which delivers a beam of high-energy (3 MeV) protons; these are focussed onto the target by an electrostatic lens (Sie & Ryan 1986). The X rays excited by the collision of the protons with the target are collected by a Si(Li) energy-dispersion detector, and recorded as X-ray spectra (Fig. 3). These spectra have very low background compared to electron-microprobe spectra; it is this feature that allows the determination of trace-element concentrations at very low levels. Peak areas are extracted from these spectra, and reduced to concentration values, as described by Ryan *et al.* (1990a,b; see also Griffin *et al.* 1988). The method is independent of standards; however, the analytical values are usually normalized to a known element (in this case, Fe) to compensate for uncertainties in the measurement of accumulated charge. This correction is typically *ca.* 10% relative. Analyses of known materials, such as glasses prepared from rock standards, demonstrate that the accuracy of the method is within the reported precision, and typically better than ±5–10% (Griffin *et al.* 1988, Ryan *et al.* 1990a,b).

To use high beam-currents, and thus achieve low detection-limits within reasonable analytical times, it is necessary to attenuate major-element X-ray lines by placing metal foils between the sample and the detector. In this work, we have used a foil of Al 300 μm thick as a filter; this effectively absorbs most of the Fe X rays, and restricts the choice of elements to those heavier than Fe. Typical beam-currents during the analysis of pyrite were 8–10 nA, giving count rates of *ca.* 1000–3000 cps, and analysis times of 6–10 minutes for an accumulated live charge of 3 μC.
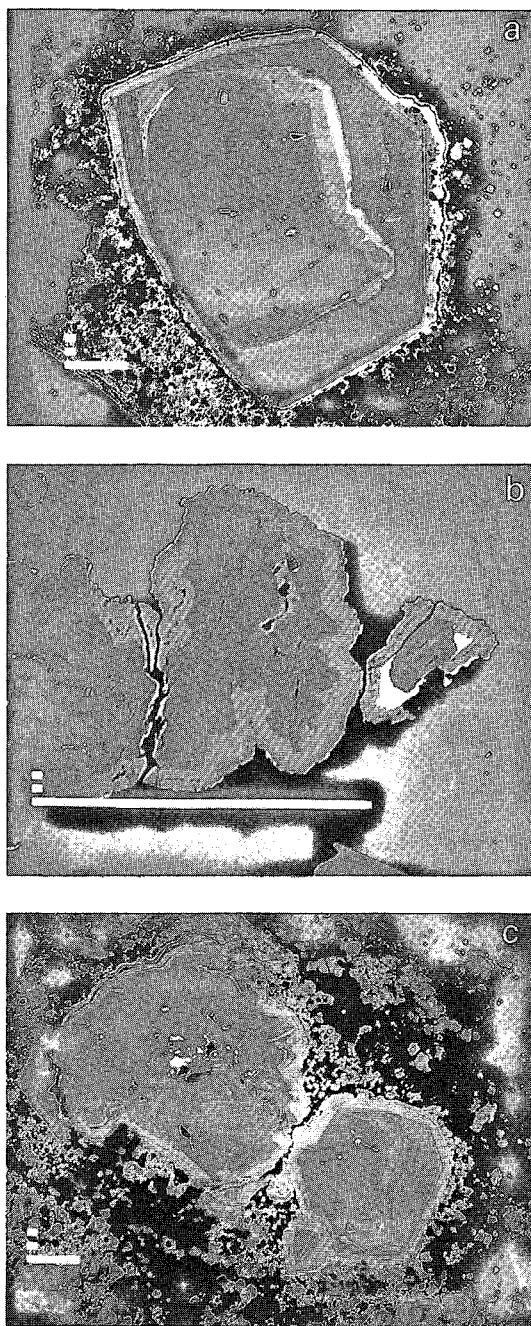
The proton beam used in these analyses typically had a diameter of 20–30 μm, and the effective maximum depth of analysis was *ca.* 20–25 μm. The volume sampled is therefore greater than in electron-microprobe analysis, and this raises the possibility of analyzing concealed subsurface inclusions. Careful back-scattered electron imaging (using the electron microprobe) of samples subsequently analyzed by proton microprobe showed that areas within the smoother-polishing pyrite are homogeneous down to the μm level and are free of microinclusions. Pitted and spongy-textured marcasite and pyrite characteristic of types B and C also have microinclusion-free domains. Therefore in most cases we are confident that proton-beam overlap onto microinclusions (at the μm scale) is not a serious problem. We are less confident of our ability to position the proton beam in specific growth-zones of the pyrite, especially in the finer-grained varieties. Some of the high-As compositions, in particular, may represent averages of more than one zone with widely different As contents; this effect may account for some of the scatter in the correlation plots shown below.

Sixteen polished sections prepared from drill core, and three pyrite concentrates from drill cuttings, have been analyzed, and over 160 point analyses were carried out. Samples were selected to provide spatial coverage of the deposit (Fig. 1) and to be representative of a range of precious metal contents. Drill-core intervals from which microprobe samples were taken, as well as hand specimens collected underground, were analyzed for Au and Ag to determine whether the trace-element chemistry of pyrite can be correlated with precious metal values in the whole-rock samples. Samples were grouped into classes of "mineralized" (Au + Ag > 7 ppm, Au > 1 ppm), "weakly mineralized" (Au + Ag 2–7 ppm, Au 0.1–1 ppm) and "barren" (Au + Ag < 2 ppm, Au < 0.1 ppm).

Results

The analyzed grains of pyrite and marcasite show a very wide range in As content, from < 100 ppm to > 7 wt.% (Fig. 4); much of this variation can be found within single polished sections and even within single grains. To provide a more coherent view of the data, we have grouped the analyses: (a) by bulk

FIG. 2. BSE images of Fe sulfide minerals from the North Arm deposit. a. Subhedral (type A) pyrite in sample 820878, with cryptic zoning defined by variations in As content. Note truncated growth-zoning and overgrowth by rim of type-C arsenian pyrite, which also occurs in fine-grained aggregates in the surrounding quartz. Scale bar = 100 μm. b. Marcasite cores with internal pitted and bladed pseudomorphs showing epitaxic overgrowths of cryptically zoned type-C arsenian pyrite. White phase overgrowing marcasite in small grain on right is arsenopyrite. Sample 820869; scale bar = 100 μm. c. Subhedral grain and complex aggregate of type-A pyrite containing tiny inclusions of electrum (white). This pyrite shows cryptic and truncated growth-zones defined by variation in As content. It is overgrown and surrounded by fine-grained cryptically zoned type-C arsenian pyrite. Sample 820878; scale bar = 100 μm.
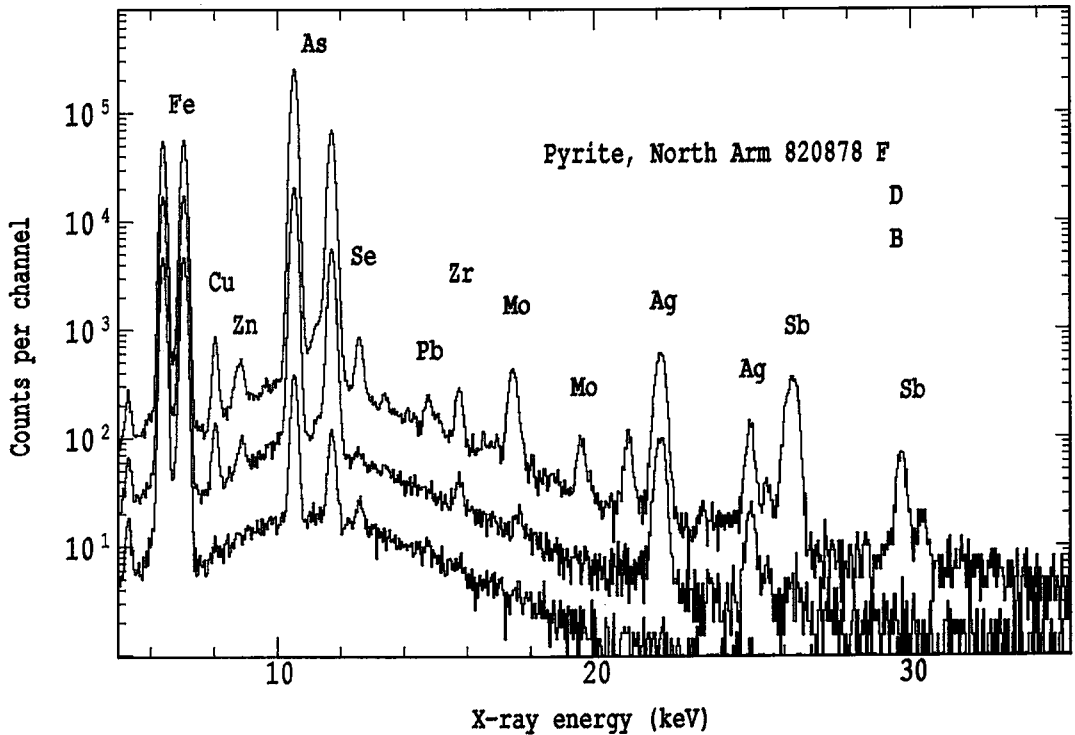
FIG. 3. PIXE spectra of three pyrite grains of varying As content in sample 820878.

content of precious metals, and (b) by As content, using the histogram shown in Figure 4 to define "natural" groupings. The spectra for points falling within a particular arsenic-content group in each sample were screened to reject several with extremely high values of Pb or Zn, on the suspicion that these had sampled subsurface inclusions of galena or sphalerite. The remaining spectra were then summed digitally, to produce a composite spectrum with better statistics and lower detection-limits. The analyses of representative summed spectra, and of some individual points, are presented in Table 1. Table 2 shows average values of several elements in each sample, grouped according to their precious-metal content as described above.

Most of the points analyzed contain significant levels of Cu, As, Se, Ag and Sb (Table 1). Elements sought, but not found, include: Ni [typical MDL (minimum detection limit, 99% confidence) = 50 ppm], Pd (5 ppm), Pt (15 ppm), Au (15 ppm), Cd (5 ppm), In (7 ppm), Sn (6 ppm). Au was not detected, even in grains containing inclusions of electrum. Zn, Mo, Pb, Hg and Tl were detected at significant levels at several of the analyzed points. Detection limits for Hg and Tl are relatively high because of interference by the low-energy tail on the As$K\alpha$ peak and by the $K\beta$ peaks of As and Se.

Molybdenite, sphalerite and galena have been observed in some samples, and small inclusions below the polished surface may have been sampled by the beam in these cases, accounting for the Zn, Mo and Pb, and some of the Ag and Cu. However, these elements are, like most others, enriched in high-As samples, and there is no *a priori* reason to doubt that they also reside in the pyrite.

Coexisting pyrite and marcasite were analyzed in several samples. No consistent differences in trace-element composition were found between the phases, except for Ag. Values for Ag in marcasite overlap those for pyrite in the same samples, but the arithmetic means are consistently lower in the marcasite.

As noted above, many samples contain grains of pyrite that show complex zoning. Point traverses across such grains illustrate the covariation of elements such as Ag and Se, and Cu and As (Fig. 5). The highest contents of most trace elements are typically found in high-As pyrite, especially the fine-grained type-C pyrite. However, the correlations of these elements with As show considerable variation in detail, and more than one type of correlation trend is commonly seen in a single sample (Fig. 6). These trends also are observed in the data set as a whole, using the summed spectra (Figs. 7–10).

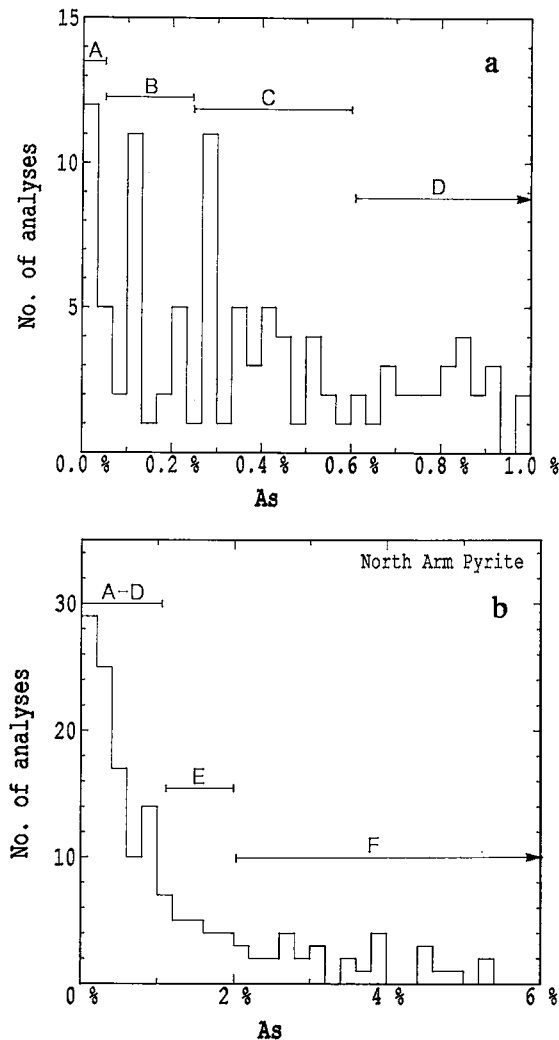Antimony is broadly correlated with As (Fig. 7a).

FIG. 4. Histogram showing distribution of As in point analyses collected in this study. Groupings used for summed spectra are indicated by horizontal lines labeled A, B, etc.

In the summed spectra, selenium shows a poor overall correlation with As; however, the majority of the samples (22 of 33) lie near a line corresponding to As/Se = 400 (Fig. 7b). A more striking correlation is shown by the results of individual point-analyses (Fig. 6a). A plot of Se *versus* Sb (Fig. 7c) shows a broad scatter between Sb/Se ratios of 0.25 and 15.

Silver is poorly correlated with As; some high-As samples contain little Ag, and *vice versa* (Figs. 6b, 8a). High-Ag, low-As point analyses may be the result of contamination by subsurface grains of electrum or naumannite. A plot of Ag *versus* Se (Fig. 8b) shows three broad trends. A plot of Ag *versus* Sb (not shown) is broadly similar.

Copper shows a good correlation with As (Fig. 9a). A Cu–Ag plot (Fig. 9b) shows two distinct trends, one with Ag/Cu $\approx$ 0 and the other with Ag/Cu $\approx$ 1; there are few intermediate points. The Cu–Sb plot (Fig. 9c) is very similar to the Cu–Ag plot; it shows a broad positive correlation, with Cu/Sb $\approx$ 0.25, and a trend of increasing Cu without Sb; the Cu–Se plot (not shown) is similar.

Mercury is found at significant levels almost exclusively in high-As samples (groups D–F); it shows a broad positive correlation with As. Tl was detected only in the high-As pyrite of sample 820895 (Table 1). Molybdenum also occurs only in high-As samples (> 1000 ppm As), and shows a broad positive correlation with As; however, many high-As points contain no Mo. Zn shows little correlation with As, and the same is true of Pb; this suggests that these elements may occur, at least in part, as submicroscopic inclusions in the pyrite.

The strong relationship among Cu, Ag, Sb and As is demonstrated in Figure 10. Normalization to Sb results in strong linear correlations between log (Cu + Ag) and As, which suggests a mixing relationship. Cu/Sb (atomic) ratios are essentially bimodal, centering on values of *ca.* 0.8 (similar to observed freibergite; Ashley 1987) and 5.5, with some higher values. High contents of Ag are most common in samples with the lowest Cu/Sb ratio (Fig. 10c).

The mean compositions of the analyzed pyrite in each sample, grouped according to precious-metal content of the bulk sample, are shown in Table 2 and Figure 11. The contents of Ag, Sb and Se show a broad relation to grade; no such relation is obvious for As or Cu.

DISCUSSION

Arsenic in pyrite

The presence of significant amounts of As in pyrite, especially from epithermal deposits, has been noted by many authors (*e.g.*, Christiansen *et al.* 1983, Hulen & Nielsen 1986, Glaser 1986, Fleming *et al.* 1986, Ballantyne & Moore 1988, Fleet *et al.* 1989). This presents a problem, because substantial solid-solution of arsenic in pyrite has not been demonstrated experimentally; Clark (1960) reported a maximum As content of 0.5% in pyrite in equilibrium with arsenopyrite at 600°C. This lack of extensive solid-solution is consistent with the large differences in crystal structure between pyrite and arsenopyrite.

Fleet *et al.* (1989) reported up to 8.4% As in zoned pyrite from hydrothermal gold deposits. Assuming Clark's (1960) results to be correct, Fleet *et al.* (1989) suggested that As is incorporated as a metastable solid-solution in pyrite, and that the process may be controlled by surface chemistry. Ballantyne & Moore (1988), after rejecting alternative hypotheses, con-

TABLE 1. REPRESENTATIVE COMPOSITIONS OF PYRITE

sample	820367	820367	820367	820367	820435	820435	820435	820435
*class	A	B	C	D	A	B	C	D
#type	qtz. vein	qtz. vein	qtz. vein	qtz. vein	dissem.	dissem.	dissem.	dissem.
no. ana	3	5	4	2	2	3	6	1
Cu	50±5	48±3	93±5	150±16	<22	31±5	48±3	133±10
Zn	<10	<8	<10	<15	<13	<11	<8	<20
As	158±3	1620±30	3420±70	9860±220	149±5	1200±20	2810±50	7100±100
Se	72±2	95±2	83±2	106±3	45±2	31±2	24±2	<8
Mo	14±2	6±1	12±1	42±2	<4	<3	<2	<6
Ag	30±2	75±2	139±4	33±3	84±5	41±2	46±2	32±3
Sb	23±3	21±3	16±3	25±4	12±3	<10	<7	<16
Au	<13	<11	<12	<19	<16	<13	<10	<25
Hg	<13	<10	<12	<18	<16	<13	<9	36±7
Tl	<11	<9	<10	<16	<13	<11	<8	<23
Pb	16±3	<9	<10	125±55	<13	<11	<8	<20

sample	820550	820550	820550	820550	820878	820878	820878	820878
class	B	C	D	F	B	C	D	E
type	dissem.	dissem.	dissem.	dissem.	dissem.	dissem.	dissem.	dissem.
no. ana	2	2	2	2	2	6	3	1
Cu	50±6	99±10	303±12	413±27	<22	52±4	184±7	280±18
Zn	<13	<15	<14	17±4	<13	<8	<12	<22
As	1170±20	3290±80	1.2%±0.1	2.3%±0.1	546±11	3910±50	8340±130	1.8%±0.1
Se	20±2	8±2	10±4	30±10	<5	67±2	29±5	57±10
Mo	<4	<4	<4	9±2	<4	<3	<4	<6
Ag	26±3	21±3	65±5	18±4	7±2	580±12	219±6	<8
Sb	13±3	35±7	118±8	32±5	<11	14±3	24±4	<17
Au	<17	<20	<18	<18	<17	<10	<16	<30
Hg	<16	<19	<17	<18	<16	<10	<15	57±14
Tl	<14	<17	<15	<16	<14	<9	<13	<25
Pb	16±10	291±37	267±57	50±40	44±8	<9	<12	<24

sample	820878	820895	820895	820895	820896	820896	820896	820896
class	F	D	E	F	A	B	C	D
type	dissem.	breccia	breccia	breccia	qtz. vein	qtz. vein	qtz. vein	qtz. vein
no. ana	5	2	4	3	2	2	3	1
Cu	344±30	125±13	201±15	618±48	23±5	34±7	68±5	60±8
Zn	31±4	<15	26±3	79±10	<13	<13	<11	<19
As	3.2%±0.1	8390±95	1.5%±0.1	6.0%±0.1	271±5	2020±40	3990±70	6370±80
Se	115±13	21±2	46±6	80±25	<5	9±2	11±2	16±5
Mo	86±2	143±4	68±2	136±3	<4	<4	<4	<6
Ag	402±8	24±3	20±2	23±3	<6	9±3	11±2	<8
Sb	748±25	415±13	924±25	1600±40	294±13	91±7	92±5	59±9
Au	<13	<19	<14	<21	<16	<17	<14	<25
Hg	<13	29±9	93±7	232±23	16±4	<16	<13	28±7
Tl	<12	<16	87±24	169±66	<13	<14	<11	<21
Pb	131±66	225±30	111±36	<18	<13	<14	<11	<20

* Classes defined on As content: see Fig. 4. Concentrations in ppm unless noted.
\# Pyrite/marcasite from quartz veins or breccia-fillings, or disseminated in altered wallrock

TABLE 2. MEAN CONCENTRATIONS OF TRACE ELEMENTS IN PYRITE (ppm)

Sample	n	Cu	Zn	As	Se	Mo	Ag	Sb	Hg	Pb	Tl
Mineralized Samples											
820435 py	14	43	<	2220	37	<	217	<	<	42	n.a.
20/56-58 py	3	642	<	5570	28	<	656	89	22	918	n.a.
820367 mc	4	92	<	3080	116	29	69	44	<	40	<
820367 py	10	68	<	2950	76	10	85	11	<	<	<
820886 py	6	245	36	12400	110	8	137	408	48	77	<
820878 py	20	218	<	18900	85	<	410	591	70	152	n.a.
29/22-24 py	5	150	<	1520	9	28	68	307	28	235	<
820869 py	10	539	48	35100	106	205	625	1250	137	169	<
820869 mc	1	206	<	10500	87	415	465	1470	55	157	<
820413 py	8	371	45	15600	50	25	193	995	82	496	<
Mean	81	231		12800	71		293	472	42	172	
Weakly Mineralized Samples											
820875 py	6	113	41	4020	<	<	37	35	<	<	<
820368 mc	4	131	23	8000	23	<	89	287	25	103	n.a.
820368 py	4	304	25	22650	67	16	379	1401	227	78	n.a.
820896 py	8	46	<	2850	8	<	9	130	<	<	<
820427 py	3	29	<	2690	26	<	43	8	<	27	<
820895 py	6	335	39	31000	102	161	28	1400	212	151	54
820895 mc	3	259	32	23000	64	<	16	495	160	<	161
820550 py	8	218	<	9860	31	<	33	48	25	144	<
29/56-58 py	6	105	54	3620	13	7	49	50	<	381	<
Mean	48	167		11100	34		64	387	62	107	
Barren Samples											
820392 py	5	399	42	6760	17	<	14	137	34	<	<
820548 py	9	292	<	11200	27	<	50	115	23	780	<
820871 py	4	141	<	5640	10	<	10	129	<	490	<
820884 py	3	410	<	19600	53	<	66	123	43	494	<
Mean	21	305		10300	25		36	124	24	498	

< : Below the detection limit for more than half the population analyzed. Values < MDL treated as zero.
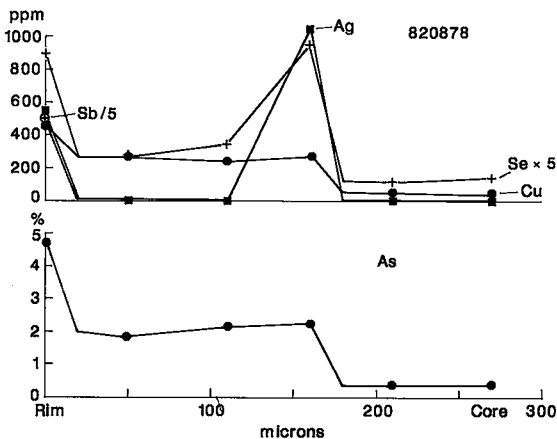

FIG. 5. Concentration of some elements along a point traverse from core to rim, across the pyrite grain shown in Figure 2a.

cluded that high levels of As in epithermal pyrite might result from micro-scale irreversible reactions, involving local redox reactions and the disequilibrium solution of FeAsS in pyrite.

The data presented here indicate that most of the other trace elements in pyrite from North Arm are associated at least in a general way with arsenic. This association may be understandable in terms of a precipitation mechanism such as that proposed by Ballantyne & Moore (1988). Disequilibrium incorporation of As into the pyrite structure would lead to distortion of the structure and a large number of defects; these would provide sites for other minor elements that do not normally enter the pyrite structure. An alternative is that arsenopyrite is actually deposited as a discrete phase on the surface of the pyrite. Fleet *et al.* (1989) have described layers *ca.* 10 Å thick of a marcasite-like phase in high-As pyrite; these lamellae occur along stacking faults in the pyrite. The marcasite-like phase could be arsenopyrite, in which case the lamellae could represent exsolution of arsenopyrite from a metastable high-As pyrite. However, they might also be interpreted as growth layers.

The interelement correlations observed in pyrite from North Arm (Figs. 7–11) suggest mixing lines, and imply that most of the trace elements in the pyrite may be located in distinct occluded phases, rather than in the pyrite structure. Starling *et al.* (1989), following Bancroft and coworkers (Jean &

Bancroft 1985, Hyland & Bancroft 1989) have suggested that the conducting properties of surfaces are important in promoting the observed precipitation of submicroscopic grains of reduced phases, such as native Au, Ag, Te, and polymetallic phases on the surface of pyrite grains. The proposed mechanism involves the adsorption of chloride or thiosulfide complexes at sites of defects on the pyrite surfaces, followed by reduction using electrons provided by the pyrite. Arsenian pyrite typically is a p-type semiconductor (Pridmore & Shuey 1976), and pyrite with As > Cu + Hg, etc., generally shows high conductivity. P-type defects, such as those provided by As, trap electrons, which thus become available for the reduction of metal-bearing complexes. The process would be enhanced by the high electrical conductivity shown by arsenian pyrite.

A mechanism similar to that proposed by Starling et al. (1989), but involving the precipitation of phases such as sulfosalts, arsenopyrite, electrum, naumannite and allargentum, can explain the overall association of Cu, Sb, Se and, to a lesser extent, Ag with As in pyrite from North Arm. The correlations shown in Figure 10 are qualitatively consistent with mixing between a sulfosalt phase of the type $(Fe,Cu,Ag)_{12}(As,Sb)_4S_{13}$, arsenopyrite, and pyrite. The As/Sb ratio essentially measures the arsenopyrite/sulfosalt ratio, whereas the Cu/Sb ratio reflects the composition of the sulfosalt. The correlation of Cu/Sb with As/Sb (Fig. 10a) suggests that in the more As-rich samples of pyrite, the sulfosalt phase is also generally more arsenian (i.e., greater tennantite component). Scatter in the Cu/Sb ratios also will be produced by substitution of Fe and Ag (cf. Fig. 10c).

This three-phase mixing can explain most of the observed variation in the minor and trace elements; similar microinclusions of native Ag or naumannite can explain the few points with anomalously high Ag. The involvement of several precipitate phases could produce some scatter and the appearance of more than one trend on several of the figures. In samples 820869, 820878 and 820895, for which the largest numbers of high-As points were analyzed, the broad Sb–As and Ag–As correlations intersect the As axis at 1–2% As (Figs. 7, 8). This may define the level of As that is actually resident in the pyrite structure in these specimens.

The model suggested here can be tested by high-resolution TEM studies designed to image inclusions on the nanometer scale (cf. Fleet et al. 1989), and by detailed crystallographic studies of high- and low-As zones in single pyrite grains. These studies are unfortunately beyond the scope of this work.

Causes of zoning in pyrite

The zoning of As (and other elements) in the pyrite from North Arm is similar to Fe zoning in sphalerite
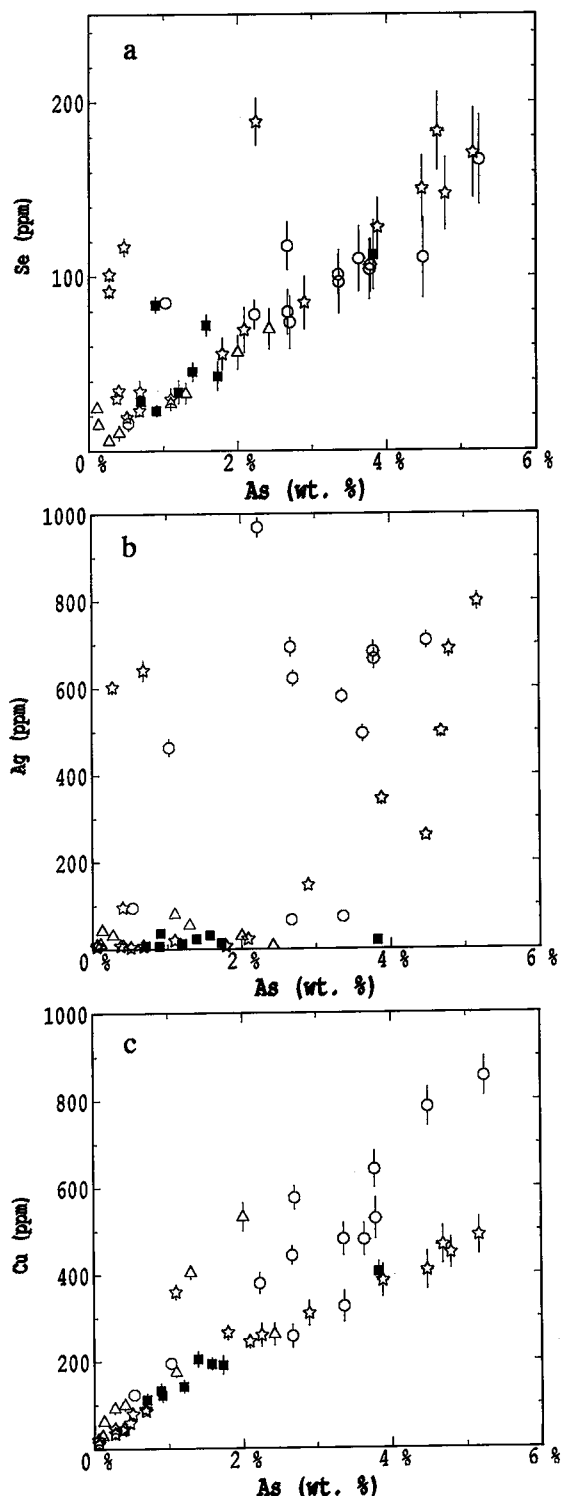

FIG. 6. Element correlations in point analyses of pyrite from four samples. Circles, 820869; squares, 820895; triangles, 820550; stars, 820878.
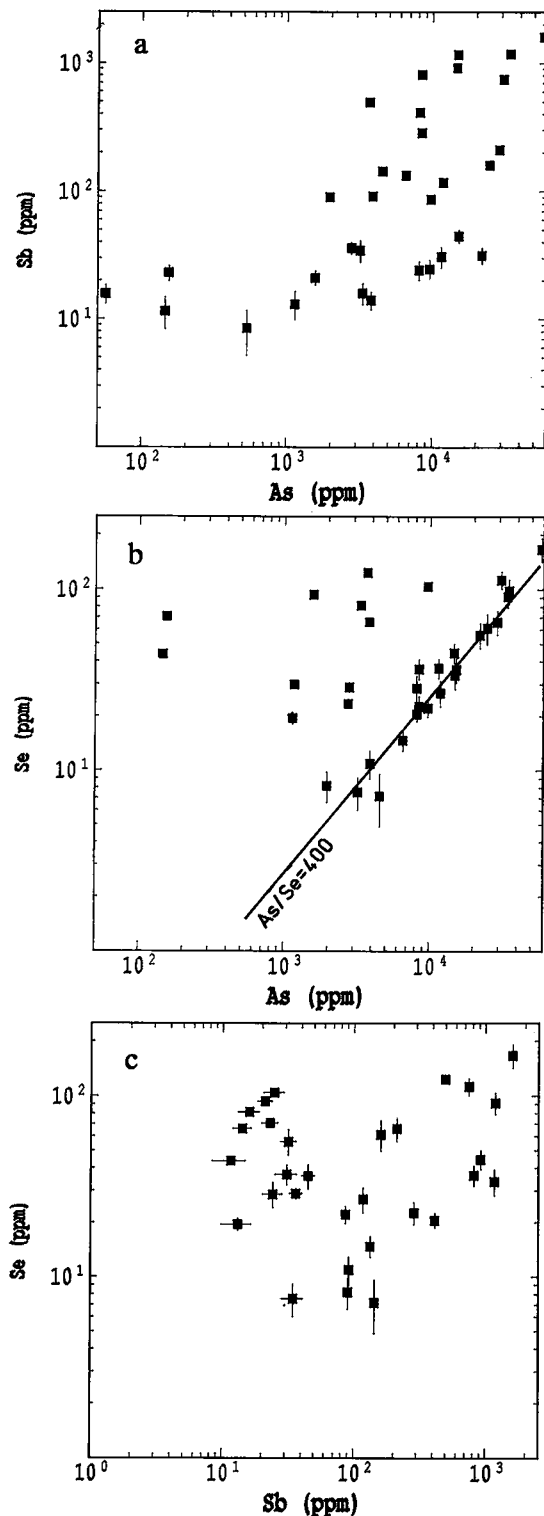
FIG. 7. As–Sb–Se relations in pyrite (summed spectra); data from Table 1.

from epithermal, VMS-type and Mississippi-Valley-type ore deposits (Barton et al. 1977, McLimans et al. 1980, Barton & Bethke 1987). In sphalerite, this zoning is generally interpreted as due to episodic variations in fluid composition, e.g., in the activities of Fe, S, O and in pH. By analogy, other studies of As zoning in pyrite (e.g., Fleet et al. 1989) have suggested that the zoning reflects rapid (relative to rates of crystal growth) variations in the As content of mineralizing fluids through time.

In their study of the geochemistry of arsenic in geothermal systems, Ballantyne & Moore (1988) showed that the arsenic content of hydrothermal fluids is inversely proportional to $P(H_2S)$. The North Arm hydrothermal system was relatively shallow, and repeated boiling is manifested in hydrothermal breccias, and in the characteristics of mineralized veins and fluid inclusions (Ashley & Andrew 1990). In such a system, rapid variations in pressure, from hydrostatic to lithostatic, could have been caused by fracturing and resealing of fluid conduits. These variations, and the accompanying boiling, could also produce rapid variations in pH and the activity of S, and thus in the solubility of arsenic in the fluids. Spycher & Reed (1989) argued that As largely remains in the fluid phase during boiling. Boiling processes might therefore account for the alternate deposition of pyrite and arsenopyrite, or of low- and high-As pyrite. However, to explain the fine-scale zoning in the pyrite, this process would have to operate in an oscillatory fashion, with cycle times being rapid relative to rates of crystal growth.

However, large changes in the fluid composition, corresponding to each individual band, may not be required. Jamtveit (1991) presented a detailed analysis of oscillatory growth-zoning in andradite-grossular garnet from low-temperature hydrothermal veins, and argued that the boundaries of individual bands are phase contacts, representing compositions on either side of a solvus. The patterns of zoning, as expressed by band widths and the frequency of reversals, are fractal in nature, and can be modeled in terms of non-linear dynamic (chaos) theory. Jamtveit concluded that in systems controlled by a solvus, chaotic oscillatory patterns, involving alternate deposition of the phases on either side of the solvus, can be produced by relatively minute changes in external factors.

Our data are compatible with the deposition of submicroscopic grains of arsenopyrite (and a sulfosalt phase) on the growing surfaces, and Clark's (1960) experimental work is consistent with a solvus between pyrite and arsenopyrite. Jamtveit's model suggests that the oscillatory zoning in pyrite such as that described here might reflect rapid and chaotic changes in the free energy of the pyrite–arsenopyrite system on a very local scale, rather than larger-scale changes in the As activity in the fluid. Further detailed analysis of such zoning, and TEM studies
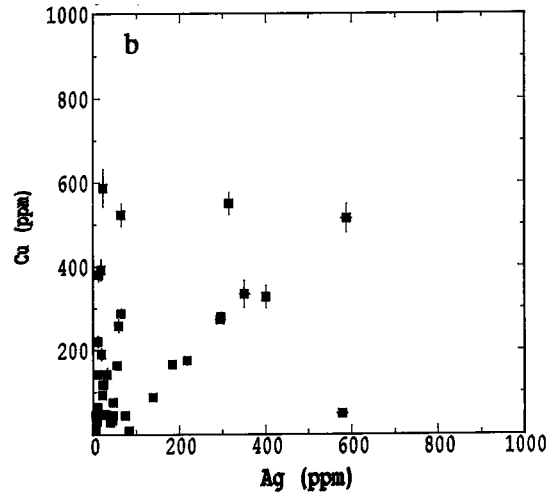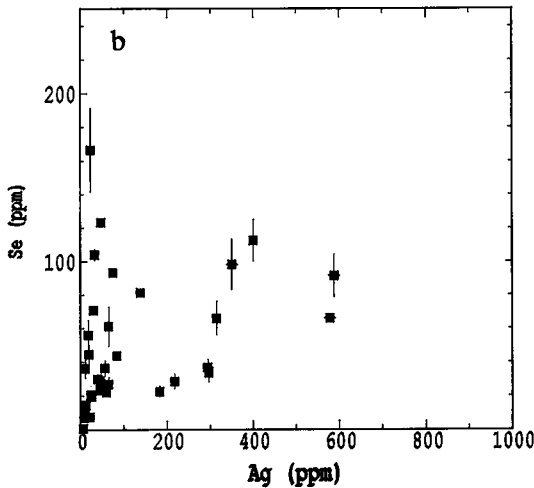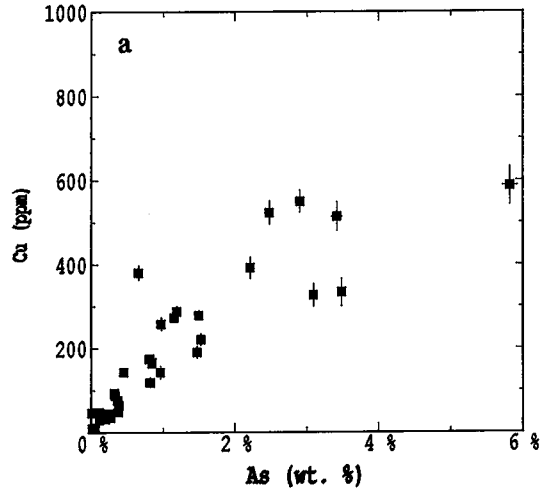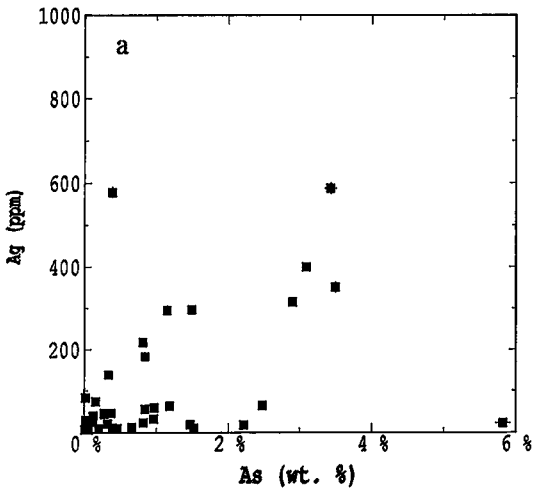
FIG. 8. Ag–As–Se relations in pyrite (summed spectra); data from Table 1.

of the pyrite, clearly are necessary to test this model.

If submicroscopic inclusions of a sulfosalt phase are largely responsible for the Ag, Cu, Sb and Se contents of the analyzed pyrite, then the groupings of Cu/Sb, Se/Sb, Ag/Cu, Ag/Sb and Ag/Se ratios described above may reflect different generations of mineralization, or larger fluctuations in environmental conditions during the evolution of the North Arm hydrothermal system, which have produced changes in the chemistry of this phase.

Gold in pyrite

Despite the presence of electrum as a free phase and as inclusions in pyrite, the pyrite from North Arm does not have measureable (> 10 ppm) gold contents. In this respect it differs from the pyrite of
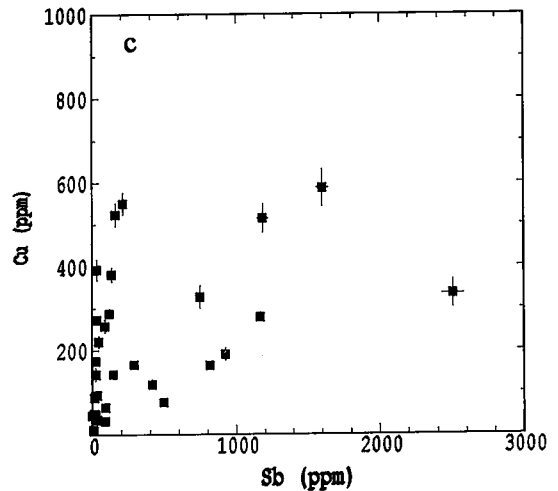

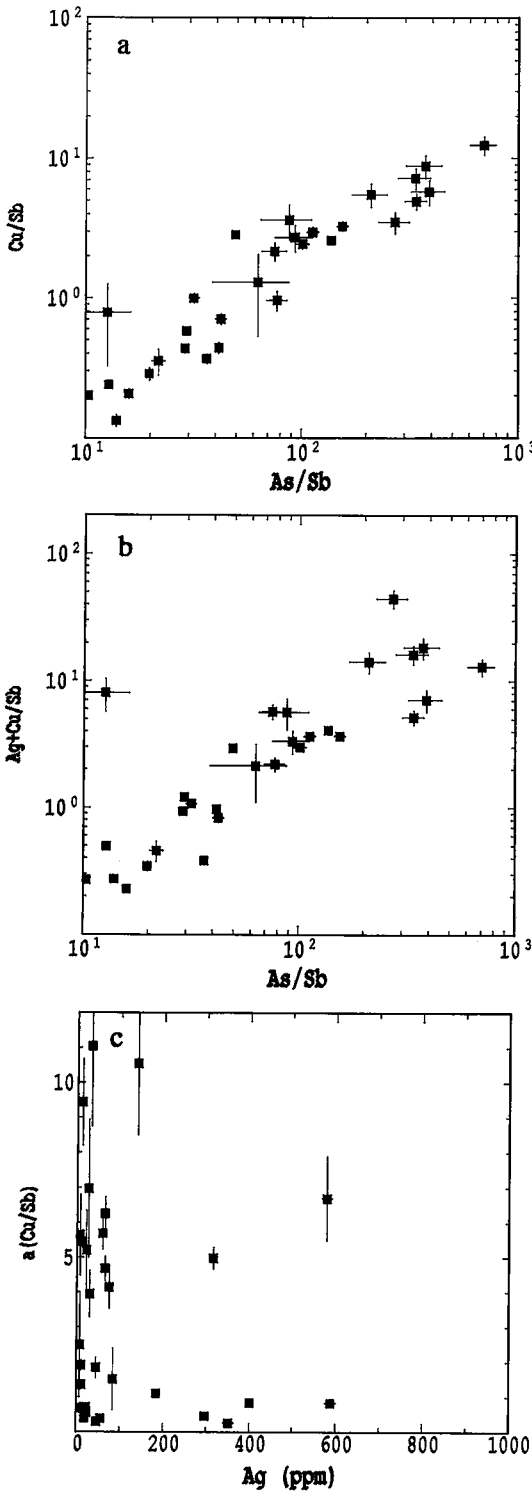FIG. 9. Cu–Ag–Sb relations in pyrite (summed spectra); data from Table 1.

FIG. 10. Cu–Ag–Sb–As relations in pyrite (summed spectra); data from Table 1.
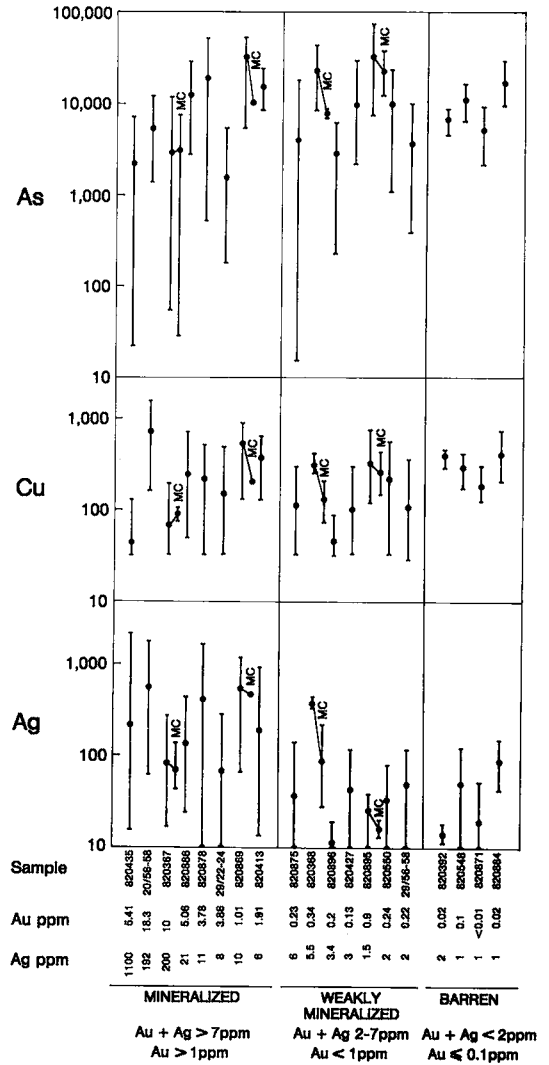

FIG. 11. As, Cu and Ag variations in pyrite and marcasite from the North Arm deposit in relation to bulk sample Au and Ag content. Bars represent ranges of elements detected in individual samples, black dots, the arithmetic means. MC signifies ranges for marcasite; remainder are for pyrite. Tie lines connect means of pyrite and marcasite from each sample. Element contents are in parts per million.

some other epithermal deposits, such as the Emperor deposit of Fiji, which contains up to 4000 ppm Au (Ahmad *et al.* 1987, Griffin, unpubl. data). Cook & Chryssoulis (1990) have documented Au contents of up to 110 ppm in pyrite from several deposits, using ion-microprobe techniques. The models proposed by Starling *et al.* (1989), Jean & Bancroft (1985) and Hyland & Bancroft (1989) were originally devised to explain the precipitation of native gold

onto pyrite surfaces. It is therefore reasonable to ask why Au precipitation has not occurred at North Arm.

Jean & Bancroft (1985) found that whereas chemisorption–reduction processes would precipitate native gold on pyrite surfaces from $AuCl_4^-$ solutions, this did not occur in AuCN solutions. They explained this by reference to the standard redox potentials for the two systems; a strongly reducing surface would be needed to reduce AuCN. Though further data are clearly necessary, we suggest that the failure of Au to precipitate onto the surface of arsenian pyrite at North Arm reflects the mechanism by which gold was transported in this system. Fluid inclusion and mineralogical data (Ashley & Andrew 1990) indicate that the mineralizing fluid was dilute (low-Cl), and that deposition temperatures averaged *ca.* 270°C. Under these circumstances, transport of Au was probably dominated by the bisulfide complex (Seward 1989). Further comparative studies of pyrite geochemistry in different types of epithermal systems may yield useful data on the geochemistry of precious-metal transport.

Pyrite geochemistry as a guide to mineralization

The data in Table 2 and Figure 11 suggest that pyrite geochemistry is not a good guide to Au–Ag mineralization in the North Arm deposit. Whereas there is a broad increase in the average or maximum Ag, Sb and Se contents of pyrite with increasing grade (as measured by assay of core sections), there is little in the pyrite of weakly mineralized samples to indicate proximity to high-grade zones. We have not been able to recognize any systematic variation in the chemistry of pyrite near mineralized zones, even within single drill-cores.

The reasons for this poor correlation are probably to be found in the detailed structure of the North Arm deposit. Most samples contain several generations of pyrite, with quite different trace-element chemistry, and Au–Ag mineralization may be connected only with one or a few of these. In vein-stockwork systems such as the North Arm deposit, and probably in other epithermal deposits, precious-metal mineralization may be closely related only to specific sets of fractures formed at specific times; pyrite formation may be much more pervasive and may have extended over longer times. It is therefore perhaps unlikely that the geochemistry of the specific episodes during which precious metals were deposited will be pervasively reflected in the chemistry of pyrite formed nearby, but in other episodes of mineralization.

The data from North Arm indicate no significant difference in the As content of pyrite in mineralized and barren samples. The distribution of arsenic in primary and secondary dispersion-haloes around the deposit probably is related mainly to the modal abundance of pyrite. In this particular case, the haloes defined by bulk geochemistry appear to be more useful in defining drilling targets than data on pyrite geochemistry. However, the geochemistry of pyrite, and particularly the details of patterns of zoning in the pyrite, preserve significant information about the chemical and physical conditions of deposit formation. Such information will be important for modeling of the deeper zones of such deposits, and ultimately in guiding exploration strategies in epithermal and mesothermal systems.

REFERENCES

AHMAD, M., SOLOMON, M. & WALSHE, J.L. (1987): Mineralogical and geochemical studies of the Emperor gold telluride deposit, Fiji. *Econ. Geol.* **82**, 345-370.

ASHLEY, P.M. (1987): Sulphide–selenide–metal alloy association at North Arm epithermal precious metal prospect, Queensland, Australia. *Trans. Inst. Min. Metall.* **96**, B221-227.

_____ & ANDREW, A.S. (1990): Contrasting alteration styles associated with epithermal mineralisation, North Arm Volcanics, Queensland. *Geol. Soc. Aust., Abstr.* **25**, 23-24.

BALLANTYNE, J.M. & MOORE, J.N. (1988): Arsenic geochemistry in geothermal systems. *Geochim. Cosmochim. Acta* **52**, 475-483.

BARTON, P.B., JR. & BETHKE, P.M. (1987): Chalcopyrite disease in sphalerite: pathology and epidemiology. *Am. Mineral.* **72**, 451-467.

_____, _____ & ROEDDER, E. (1977): Environment of ore deposition in the Creede mining district, San Juan Mountains, Colorado. III. Progress toward interpretation of the chemistry of the ore-forming fluid for the OH vein. *Econ. Geol.* **72**, 1-24.

CABRI, L.J., CHRYSSOULIS, S.L., DE VILLIERS, J.P.R., LAFLAMME, J.H.G. & BUSECK, P.R. (1989): The nature of "invisible" gold in arsenopyrite. *Can. Mineral.* **27**, 353-362.

CHRISTIANSEN, O.D., CAPUANO, R.A. & MOORE, J.N. (1983): Trace element distribution in an active hydrothermal system, Roosevelt Hot Springs thermal area, Utah. *J. Volc. Geotherm. Res.* **16**, 99-129.

CLARK, L.A. (1960): The system Fe–As–S: phase relations and applications. *Econ. Geol.* **55**, 1345-1381.

COOK, N.J. & CHRYSSOULIS, S.L. (1990): Concentrations of "invisible gold" in the common sulfides. *Can. Mineral.* **28**, 1-16.

ELLIOTT, S.M. & TOWSEY, C.A. (1989): Regional drainage geochemical gold exploration techniques used in Queensland, Australia. *In* Proc. North Queensland Gold '89 Conf. (Townsville). *Aust. Inst. Min. Metall.*, Melbourne (51-62).

FLEET, M.E., MACLEAN, P.J. & BARBIER, J. (1989): Oscillatory-zoned As-bearing pyrite from stratabound and stratiform gold deposits: an indicator of ore fluid evolution. *In* The Geology of Gold Deposits: The Perspective in 1988 (R.R. Keays, W.R.H. Ramsay & D.I. Groves, eds.). *Econ. Geol., Monogr.* **6**, 356-362.

FLEMING, A.W., HANDLEY, G.A., WILLIAMS, K.L., HILLS, A.L. & CORBETT, G.J. (1986): The Porgera gold deposit, Papua New Guinea. *Econ. Geol.* **81**, 660-680.

GLASER, L.M. (1986): A new occurrence of naumannite, aguilarite and seleniferous silver sulphosalts, Wolumla goldfield, New South Wales, Australia. *Aust. Mineral.* **1**, 306-309.

GRIFFIN, W.L., JAQUES, A.L., SIE, S.H., RYAN, C.G., COUSENS, D.R. & SUTER, G.F. (1988): Conditions of diamond growth: a proton microprobe study of inclusions in West Australian diamonds. *Contrib. Mineral. Petrol.* **99**, 143-158.

HAYBA, D.O., BETHKE, P.M., HEALD, P. & FOLEY, N.K. (1985): Geologic, mineralogic, and geochemical characteristics of volcanic-hosted epithermal precious metal deposits. *In* Geology and Geochemistry of Epithermal Systems (B.R. Berger & P.M. Bethke, eds.). *Rev. Econ. Geol.* **2**, 129-167.

HEALD, P., FOLEY, N.K. & HAYBA, D.O. (1987): Comparative anatomy of volcanic-hosted epithermal deposits: acid–sulfate and adularia–sericite types. *Econ. Geol.* **82**, 1-26.

HULEN, J.B. & NIELSON, D.L. (1986): Hydrothermal alteration in the Baca geothermal system, Redondo dome, Valles caldera, New Mexico. *J. Geophys. Res.* **91**, 1867-1886.

HYLAND, M.M. & BANCROFT, G.M. (1989): An XPS study of gold deposition at low temperatures on sulphide minerals: reducing agents. *Geochim. Cosmochim. Acta* **53**, 367-372.

JAMTVEIT, B. (1991): Oscillatory zonation patterns in hydrothermal grossular-andradite garnet: nonlinear dynamics in regions of immiscibility. *Am. Mineral.* **76** (in press).

JEAN, G.E. & BANCROFT, G.M. (1985): An XPS and SEM study of gold deposition at low temperatures on sulphide mineral surfaces: concentration of gold by adsorption/reduction. *Geochim. Cosmochim. Acta* **49**, 979-987.

MCLIMANS, R.K., BARNES, H.L. & OHMOTO, H. (1980): Sphalerite stratigraphy of the Upper Mississippi Valley zinc-lead district, southwest Wisconsin. *Econ. Geol.* **75**, 351-361.

PLANT, J.A., BREWARD, N., FORREST, M.D. & SMITH, R.T. (1989): The gold pathfinder elements As, Sb and Bi – their distribution and significance in the southwest Highlands of Scotland. *Trans. Inst. Min. Metall.* **98**, B91-101.

PRIDMORE, D.F. & SHUEY, R.T. (1976): The electrical resistivity of galena, pyrite and chalcopyrite. *Am. Mineral.* **61**, 248-259.

RYAN, C.G., COUSENS, D.R., SIE, S.H. & GRIFFIN, W.L. (1990a): Quantitative analysis of PIXE spectra in geoscience applications. *Nucl. Instr. Meth.* **B49**, 271-276.

————, ————, ————, ————, SUTER, G.F. & CLAYTON, E. (1990b): Quantitative PIXE microanalysis of geological material using the CSIRO proton microprobe. *Nucl. Instr. Meth.* **B47**, 55-71.

SEWARD, T.M. (1989): The hydrothermal chemistry of gold and its implications for ore formation: boiling and conductive cooling as examples. *In* The Geology of Gold Deposits: The Perspective in 1988 (R.R. Keays, W.R.H. Ramsay, & D.I. Groves, eds.). *Econ. Geol., Monogr.* **6**, 398-404.

SIE, S.H. & RYAN, C.G. (1986): An electrostatic "Russian" quadruplet microprobe lens. *Nucl. Instr. Meth.* **B15**, 664-668.

SPRY, P.G. & GEDLINSKE, B.L. (1987): *Tables for the Determination of Common Opaque Minerals.* Econ. Geol. Publ. Co., New Haven, Connecticut.

SPYCHER, N.F. & REED, M.H. (1989): Evolution of a Broadlands-type epithermal ore fluid along alternative P–T paths: implications for the transport and deposition of base, precious, and volatile metals. *Econ. Geol.* **84**, 328-359.

STARLING, A., GILLIGAN, J.M., CARTER, A.H.C., FOSTER, R.P. & SAUNDERS, R.A. (1989): High-temperature hydrothermal precipitation of precious metals on the surface of pyrite. *Nature* **340**, 298-300.